Article **Journal of Computational Systems and ICTs**
December 2019 Vol.5 No.16 20-26

RASF and DEDR-POCS Image Fusion through Multi-layer Perceptron in SAR Imagery Systems

Fusión de imágenes RASF y DEDR-POCS a través de perceptron multicapa en sistemas SAR

YAÑEZ-VARGAS, Israel†*, QUINTANILLA-DOMÍNGUEZ, Joel and AGUILERA-GONZALEZ, Gabriel

Universidad Politécnica de Juventino Rosas, Departamento de Ingeniería Telemática, Hidalgo 102, Comunidad de Valencia, Santa Cruz de Juventino Rosas, Gto.

ID 1st Author: *Israel, Yañez-Vargas* / **ORC ID:** 0000-0001-5749-8442, **CVU CONACYT ID:** 295711

ID 1st Coauthor: *Joel, Quintanilla-Domínguez* / **ORC ID** 0000-0003-2442-2032

ID 2nd Coauthor: *Gabriel, Aguilera-Gonzalez* / **ORC ID:** 0000-0002-4160-448X

DOI: 10.35429/JCSI.2019.16.5.20.26 Received July 18, 2019; Accepted September 11, 2019

Abstract

This paper presents a novel multi-layer perceptron (MLP) based image fusion technique, which fuses two synthetic aperture radar (SAR) images, obtained from the same spatial reflectivity map, acquired with a conventional low-cost fractional synthetic aperture radar (Fr-SAR) system, enhanced via two different methodologies. The first image is enhanced using the traditional descriptive experiment design regularization (DEDR) framework through the projection onto convex solution sets (POCS) method; the second image is enhanced with the DEDR framework by incorporating the robust adaptive spatial filtering (RASF) solution operator. This work describes a MLP based technique applied to the pixel level multi-focus fusion problem characterized by the use of image windows with the idea of reducing noise and determining which pixel is clearer between the two images. Experimental results show that the proposed novel method outperforms the discrete wavelet transform based most competing approach.

Robust Adaptive Filtering, Descriptive Experiment Desing Regularization, Multi-Layer Perceptron

Resumen

Este artículo presenta una novedosa técnica de fusión de imágenes basada en perceptrón multicapa (MLP), que fusiona dos imágenes de radar de apertura sintética (SAR), obtenidas a partir del mapa de reflectividad espacial, adquiridas con un radar de apertura sintética fraccional de bajo costo convencional (Fr- Sistema SAR), mejorado a través de dos metodologías diferentes. La primera imagen se mejora utilizando el marco tradicional del diseño descriptivo de experimentos de regularización (DEDR) a través del método de proyección en conjuntos de soluciones convexas (POCS); la segunda imagen se mejora con el marco DEDR incorporando el operador de la solución robusta de filtrado espacial adaptativo (RASF). Este trabajo describe una técnica basada en MLP aplicada al problema de fusión de enfoque múltiple a nivel de píxeles caracterizada por el uso de ventanas de imagen con la idea de reducir el ruido y determinar qué píxel es más claro entre las dos imágenes. Los resultados experimentales muestran que el nuevo método propuesto tiene un mayor enfoque en la mejora de las imágenes basado en la transformación discreta de wavelet.

FIltrado Robusto Adaptivo, Diseño Descriptivo de Experimentos de Regularización, Perceptrón Multicapa

Citation: YAÑEZ-VARGAS, Israel, QUINTANILLA-DOMÍNGUEZ, Joel and AGUILERA-GONZALEZ, Gabriel. RASF and DEDR-POCS Image Fusion through Multi-layer Perceptron in SAR Imagery Systems. Journal of Computational Systems and ICTs. 2019, 5-16: 20-26.

* Correspondence to Author (email: andyeli95@gmail.com)
† Researcher contributing first author.

1. Introduction

Image fusion is generally performed at different levels of information representation, namely, pixel level, feature level, and decision level (Shutao Li & Bin Yang, 2010) . Up to now, many image fusion techniques have been developed. Basically, the fusion technique can be categorized into spatial domain fusion and transform domain fusion (Li, Yang & Hu, 2011). The spatial domain-based methods select regions from source images in the spatial domain to construct the fused image (Pajares & Manuel de la Cruz, 2004) and (Hui Li, Manjunath & Mitra, 1995).

The basic concept of the transformed domain-based methods is to perform certain multi-resolution decomposition on each source image, then integrate all these decompositions to obtain one combined representation according to some fusion rules, and finally reconstruct the fused image by performing the inverse transformation to the combined representation. Discrete Wavelet Transform (DWT) provide directional information and without carrying redundant information across different resolutions. Moreover, DWT has good locality of time frequency (Zheng et al., 2007) and (Yang et al., 2010). However, these methods based on multi-scale transforms are shift-variant; namely, their performance will quickly deteriorate when there is misregistration of the source images.

This work focuses on fusing DEDR-POCS and DEDR-RASF enhanced images. The DEDR-POCS method centers on the idea of spatial spectrum pattern (SSP) reconstruction that allows adaptive high-resolution radar image formation with speckle reduction and dynamic scene image enhancement, in the real-world uncertain operational scenarios. The RASF method enhances the image and reduces the blurring through an image filter.

These aspects are formalized by SSP estimation techniques, minimizing noise through an improved balance between resolution and noise suppression, unified by regularization tools. The idea is to compensate the different attributes that each method produces into a new fused image, balancing the performance that each method and algorithm provides.

We propose a pixel level multi-focus image fusion method based on the use of image windows and a MLP neural network, with three principal features (visibility, spatial frequency and edge detection) for classifying the information, reducing the speckle noise and determining which pixel is clearer in each image even when the image has noise and mis-registration. The rest of the paper is organized as follows. The imaging problem formalism will be described in section two, in section three we will describe the DEDR-POCS phenomenology, RASF formalism will be presented in section four, the proposed fusion method and scheme will be developed in section five, and finally in section six and seven we will describe some experiments and concluding remarks respectively.

2. Imaging Problem Formalism

Consider the numerical approximation of the imaging remote sensing (RS) system equation of observation (EO) that is represented in the vector form as (Henderson & Lewis, 1998), (Shkvarko, 2010) and (Shkvarko et al., 2011):

$$\mathbf{u}=\tilde{\mathbf{S}}\mathbf{v}+\mathbf{n}=(\mathbf{S}+\mathbf{S}_{\Delta})\mathbf{v}+\mathbf{n} \quad (1)$$

The matrix $\tilde{\mathbf{S}}=(\mathbf{S}+\mathbf{S}_{\Delta})$ represents the discrete-form approximation of the uncertain signal formation operator (SFO) function kernel with $\mathbf{S}=\langle\tilde{\mathbf{S}}\rangle$ representing the regular SFO $\Delta_{\mathbf{S}}$ and representing the zero mean random SFO perturbation term, respectively. Here, **v, n, u** are random zero-mean vectors composed of the decomposition coefficients $\{v_k\}_{k=1}^{K}$, $\{n_m\}_{m=1}^{M}$ and $\{u_m\}_{m=1}^{M}$, respectively (Li et al., 2011) characterized by the correlation matrices, $\mathbf{R_v}=\mathbf{D(b)}=\mathbf{diag(b)}$, $\mathbf{R_n}=\mathbf{N_0I}$, and $\mathbf{R_u}=\langle\tilde{\mathbf{S}}\mathbf{R_v}\tilde{\mathbf{S}}^{+}\rangle+\mathbf{R_n}$, correspondingly, where <·> defines the averaging over the randomness of the SFO, superscript $^{+}$ stands for Hermitian conjugate, and $\mathbf{N_0}$ is the power of the white observation noise vector **n**. Vector **b** is referred to as a vector-form representation of the SSP. The vector **b** represents the lexicographical ordering of the sensed scene $\{b_k=<|v_k|^2>\}_{k=1}^{K}$,, over the $K_x \times K_y$ pixel-framed 2-D scene $\{k_x = 1,\ldots, K_x;\ k_y = 1,\ldots, K_y;\ k = 1,\ldots, K = K_xK_y\}$ (Henderson & Lewis, 1998), (Shkvarko, 2010) and (Shkvarko et al., 2011).

ISSN 2444-5002

The nonlinear inverse problem for recovery of the SSP vector **b** from the available data recordings **u**, i.e., $\widehat{\boldsymbol{b}} = est_{strategy}\{\boldsymbol{b}|\boldsymbol{u}\}$, depends on the employed estimation strategy. In the basic DEDR-related framework (Henderson & Lewis, 1998), the original low resolution (LR) estimation of the SSP $\widehat{\boldsymbol{b}}_{\text{MSF}} = est_{\text{MSF}}\{\boldsymbol{b}|\boldsymbol{u}\}$, is performed employing the standard matched spatial filtering (MSF) processing in the positive convex cone solution set $\mathbb{B}_{(K)}$in the Euclidian space with the metric structure induced by the ℓ_2 scalar product which does not involve the image ℓ_1 type total variation (TV) norm (Shkvarko et al., 2011) and (Torres et al., 2014). Thus, the MSF estimate $\widehat{\boldsymbol{b}}_{\text{MSF}}$ is formed as a square detected output

$$\boldsymbol{g} = \widehat{\boldsymbol{b}}_{\text{MSF}} = \mathcal{P}_1(\text{SQ-DET}\{\mathbf{q}\}) = \mathcal{P}_{desp}(\{\boldsymbol{q}\}_{|\circ|^2}) \quad (2)$$

Of the complex coherent MSF imaging system $\mathbf{q} = \mathbf{S}^{+}\mathbf{u}$ post processed by the despeckling filter defined by the POCS operator $\mathcal{P}_1 = \mathcal{P}_{desp}$.

3. DEDR-POCS Phenomenology

The LR image (2) serves as an input for any HR reconstructive post processing techniques, i.e., as a zero step iteration $\widehat{\boldsymbol{b}}_{[0]} = \boldsymbol{g} = \widehat{\boldsymbol{b}}_{\text{MSF}}$. The general DEDR-POCS inspired adaptive iterative HR image enhancing approach featured in (Henderson & Lewis, 1998) and (Shkvarko, 2010) is based on the DEDR-restructured minimum variance distortion-less response (MVDR) method (Shkvarko, 2010) that implies the nonlinear adaptive iterative processing (Henderson & Lewis, 1998), (Shkvarko, 2010) and (Shkvarko et al., 2011) for HR SSP recovery in the solution space with the balanced ℓ_2 type image and its gradient map metrics that yields the implicit iterative technique (Shkvarko, 2010) and (Shkvarko et al., 2011)

$$\widehat{\boldsymbol{b}}_{[i+1]} = \widehat{\boldsymbol{b}}_{[i]} + \mathcal{P}_2\{\lambda_1[\widehat{\boldsymbol{f}}_{[i]} - \boldsymbol{\Phi}_{\boldsymbol{D}[i]}\widehat{\boldsymbol{b}}_{[i]}{}_{[i]}] \quad (3)$$
$$+\lambda_2[(\nabla^2\widehat{\boldsymbol{f}}_{[i]}) - (\nabla^2(\boldsymbol{\Phi}_{\boldsymbol{D}[i]}\widehat{\boldsymbol{b}}_{[i]}))]\}$$

Initialized by the despeckled MSF image (2). Here,

$$\widehat{\boldsymbol{f}}_{[i]} = \boldsymbol{f}(\widehat{\boldsymbol{b}}_{[i]}) = \boldsymbol{D}^2(\widehat{\boldsymbol{b}}_{[i]})\boldsymbol{g}, \quad (4)$$

$\nabla^2(\circ)$is the discrete-form Laplacian, $\mathcal{P}_2 = \mathcal{P}_{+\pi}$ defines a hard threshholding operator that at each iteration $i = 1, \ldots, I$ clips off all entries of $\widehat{\boldsymbol{b}}_{[i]}$ lower than the user specified nonnegative sparsity preserving tolerance threshold level π and $\boldsymbol{\Phi}_{\boldsymbol{D}[i]}$ represents the solution-dependent point spread function (PSF) operator

$$\boldsymbol{\Phi}_{\boldsymbol{D}[i]} = (\boldsymbol{\Psi}\boldsymbol{D}(\widehat{\boldsymbol{f}}_{[i]}) + N\boldsymbol{I}) \odot (\boldsymbol{D}(\widehat{\boldsymbol{f}}_{[i]})\boldsymbol{\Psi} + N\boldsymbol{I})^{*} \quad (5)$$

Constructed from the diagonal loaded by factor *N* composition of the regular MSF response matrix $\boldsymbol{\Psi} = \mathbf{S}^{+}\mathbf{S}$ and the solution-dependent $\boldsymbol{D}(\widehat{\boldsymbol{f}}_{[i]})$ at the current *i*th iteration step where symbol $\odot$ defines the element wise matrix product. In practical RS scenarios, the regularization factor *N* can be evaluated empirically from the speckle corrupted LR image following one of the local statistics techniques exemplified in (Henderson & Lewis, 1998). The adaptive iterative DEDR-POCS procedure (3) incorporates two regularization factors λ_1 and λ_2 that balance the corresponding discrepancy terms.

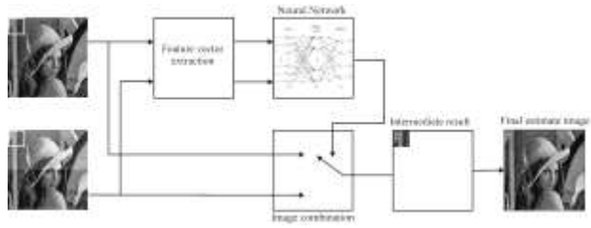

Figure 1 Schematic diagram of the proposed fusion method

The iterative process is initialized with $\widehat{\boldsymbol{b}}_{[0]} = \boldsymbol{g} = \widehat{\boldsymbol{b}}_{\text{MSF}}$ and is terminated at $\widehat{\boldsymbol{b}}_{[I]}$ for which the user specified ℓ_2-norm convergence tolerance level ε_{TL} is attained at some $i = I$. In the simulations, we specified ε_{TL} = 0.03 and treated different feasible assignments to λ_1 and λ_2 (Shkvarko, 2010) and (Shkvarko et al., 2011).

4. Robust Adaptive Spatial Filtering

The DEDR optimal SSP estimate **b**, is acquired as a solution to the nonlinear equation

$$\widehat{\boldsymbol{b}} = \mathcal{P}\{\boldsymbol{F}_{DEDR}\boldsymbol{u}\boldsymbol{u}^{+}\boldsymbol{F}_{DEDR}\}_{\text{diag}}, \quad (6)$$

Where the solution operator (SO) $\boldsymbol{F}_{DEDR}$ represents the DEDR operator in matrix-form and $\mathcal{P}$ indicates a POCS operator. The SO estimator considered in this work is the robust adaptive spatial filtering (RASF), at the same time the solution component is given by:

$$\boldsymbol{F}_{\text{DEDR}} = \boldsymbol{F}_{\text{RASF}} = \left(\boldsymbol{S}^{+}\boldsymbol{R}_{\Sigma}^{-1}\boldsymbol{S} + \widehat{\boldsymbol{D}}^{-1}\right)^{-1}\boldsymbol{S}^{+}\boldsymbol{R}_{\Sigma}^{-1}, \quad (7)$$

With $\boldsymbol{R}_{\Sigma} = \boldsymbol{R}_{\Sigma}(\beta) = (\boldsymbol{R}_{\eta} + \beta\boldsymbol{I})$ and considering $\widehat{\boldsymbol{D}} = \text{diag}(\hat{\mathbf{b}})$.

The term in $\mathcal{P}$ (6) is composed of 3 operators as follows.

$$\mathcal{P} = \mathcal{P}_3\mathcal{P}_2\mathcal{P}_1 \quad (8)$$

Where $\mathcal{P}_1 = \mathcal{P}_{desp}$ is a desplecking operator. $\mathcal{P}_2$, expresses the SAR system impulse response function separability. Finally, $\mathcal{P}_3$ represents the convergence guaranteed projector onto the nonnegative convex solution set, specified as the positivity operator $\mathcal{P}_3 = \mathcal{P}_+$, that has the effect of suppressing all negative values (Torres et al., 2014).

5. Multi-layer Perceptron Based Multifocus Image Fusion

Figure 1 shows a schematic diagram of the MLP based multi-focus image fusion proposed method. Here, we consider two source images gotten through the RASF and DEDR-POCS techniques. It is important to remark that the algorithm can be extended straightforwardly to handle more than two source images. Moreover, these images are assumed to have been registered.

5.1. Algorithm

This method first divides the initial images into windows. Given two of these windows (one from each initial image) a MLP is trained to determine which one is clearer. Then it proceeds by selecting the clearer window and constructing the final image (Li et al., 2002).

The full method is summarized as follows:

1. Divide the two initial images A and B into *M x N* windows. Denote the *i*th image window pair by A_i and B_i respectively.

2. Extract three features that reflect its clarity. Indicate the feature vectors for A_i and B_i by (SF_{Ai}, VI_{Ai}, EG_{Ai}) and (SF_{Bi}, VI_{Bi}, EG_{Bi}), respectively.

3. Design and train a MLP to determine whether A_i or B_i is clearer. The difference vector (SF_{Ai}, SF_{Bi}, VI_{Ai}, VI_{Bi}, EG_{Ai}, EG_{Bi}) is used as input, and the output is labeled according to
$\text{target}_i = \begin{cases} 1 & \text{if } A_i \text{ is clearer than } B_i, \\ 0 & \text{otherwise.} \end{cases}$

4. Validate the trained MLP on all image window pairs obtained in step 1. The *i*th window Z_i, of the fused image is then created as $Z_i = \begin{cases} A_i & \text{if out}_i > 0.5, \\ B_i & \text{otherwise,} \end{cases}$

Where out_i is the MLP output using the *i*th image window pair as input.

5. Verify the fusion result obtained in step 4. Specifically, if the MLP decides that a particular window is to come from A but with the majority of its surrounding windows taken from B, this block might be switched to come from B.

5.2. Feature vector extraction

The two *M x N* windows A_i and B_i can be fed directly into a MLP for discrimination (Li et al., 2002) and (Kulkarni, 2001).

In this paper, we extract three features from each divided image window to represent its clarity. These are the spatial frequency, visibility and an edge feature.

5.3. Spatial Frequency

Spatial frequency is used to measure the overall activity level of an image. For an *M x N* image *F*, with the gray value at Pixel position (*m*,*n*) denoted by *F*(*m*,*n*), its spatial frequency is defined as

$$SF = \sqrt{RF^2 + CF^2}, \quad (9)$$

Where RF and CF are the row frequency and column frequency respectively, the equations (10-11) represents the information for extracting information pixel by pixel and with this create a feature vector (Eskicioglu & Fisher, 1995).

ISSN 2444-5002

$$RF = \sqrt{\frac{1}{MN}\sum_{m=1}^{M}\sum_{n=2}^{N}\big(F(m,n)-F(m,n-1)\big)^2}, \quad (10)$$

$$CF = \sqrt{\frac{1}{MN}\sum_{n=1}^{N}\sum_{m=2}^{M}\big(F(m,n)-F(m-1,n)\big)^2}. \quad (11)$$

5.5. Visibility (VI)

This feature is inspired from the human visual system, and is defined as

$$VI = \sum_{m=1}^{M}\sum_{n=1}^{N}\frac{|F(m,n)-\mu|}{\mu^{\alpha+1}}, \quad (12)$$

Where μ is the mean intensity value of the image, and α is a visual constant ranging from 0.5 to 0.8 (Eskicioglu & Fisher, 1995).

5.5. Edge Features (EF)

This feature is based on the number of edges extracted from the image. Intuitively, for images of comparable complexity, a clearer image will have more edges. Here, we first apply the Canny edge detector (Eskicioglu & Fisher, 1995) to each decomposed window. The total number of one's in the resultant binary image window is then taken as the edge feature.

5.6. Neural Network Classification

Many neural networks (NN) models have been proposed for a diverse range of problems, including pattern classification. The fusion problem examined here isconsidered as a classification problem. For this paper we proposed the next idea: A feed-forward back-propagation sigmoid NN is chosen as classifier; a type of supervised NN, since a desired output is required in order to be trained. The NN model consists of a multi-layer perceptron (MLP) which uses a back-propagation learning methodology and a sigmoid activation function. The back-propagation learning method is appropriate for non-linearly-separable inputs; it is summarized as follows (Li et al., 2002) and (Eskicioglu & Fisher, 1995):

i. Select an input vector $\boldsymbol{\eta} = (\boldsymbol{\eta_1},\ldots,\boldsymbol{\eta_J})^{\boldsymbol{T}}$ and a desired output vector $\boldsymbol{d} = (\boldsymbol{\rho_1},\ldots,\boldsymbol{\rho_I})^{T}$; subscript T stands for transpose.

ii. Initialize the synaptic weights between layers $\{l = 1,\ldots,L\}$ with small random values.

iii. Compute the activation of each neuron. The activation ρ_i^l of neuron i in layer l is expressed by

$$\rho_i^l = \varphi\big(\sum_{j=1}^{J}\rho_j^{l-1}w_{ij}^l + \lambda_i^l\big),$$

Where summation is done over all Jneurons in the$(l-1)$layer, and $\varphi(\cdot)$is the sigmoid activation function. The weight for the connection from the$j$neuron in the $(l-1)$ layer to the i neuron in the l layer is denoted by w_{ij}^l; the bias of the i neuron in layer$l$ is represented by λ_i^l.

iv. Find the error between the layer Loutput vector $\boldsymbol{\rho}$ and the target vector $\boldsymbol{d}$ via $E = \frac{1}{2}\sum_{i=1}^{I}(\boldsymbol{\rho}_i - \boldsymbol{d}_i)^2$.

The calculated error is then propagated backward in order to obtain the change in the synaptic weights between layers $\{l = 1,\ldots,L\}$, through $\Delta w_{ij}^l = -\alpha\frac{\partial E}{\partial w_{ij}^l}$, where α is a training rate coefficient [12].

v. Update the synaptic weights using
$$w_{ij}^l{}_{[m+1]} = w_{ij}^l{}_{[m]} + \Delta w_{ij}^l;$$

Where $\{m = 1,\ldots,M\}$are the iterations required for achieving the desired NN output.

6. Experiments

In this section, we first experimentally demonstrate the effectiveness of the three features, proposed in the previous section (namely SF; VI and EF), in representing the clarity level of an image. An image block of size 64x 64 is extracted from the ''Lena'' image Figure 1. The figure shows two degraded versions of the same image, the first one with Gaussian noise in the up part and second one is degraded with speckle noise in the down part, this process represents the additive and multiplicative noise in RS imagery. After extracting and classifying the features, the algorithm provides an image without noise in Figure 1 (final image estimate). This suggests that all three features can be used to represent image clarity and classify the features in order to reduce the noise in the fused image.

ISSN 2444-5002

7. Simulations and Concluding Remarks

An experiment is performed on an image of size 512x512. Image windows of size 8x8 are used. Two regions, each containing 2048 image window pairs, are selected from the two DEDR-POCS and RASF images. A training set with a total of 4096 image window pairs is thus formed. The three features, SF, VI and EF, are extracted (with α=0.5 in (12)) and normalized to the range [0, 1] before feeding into the MLP.

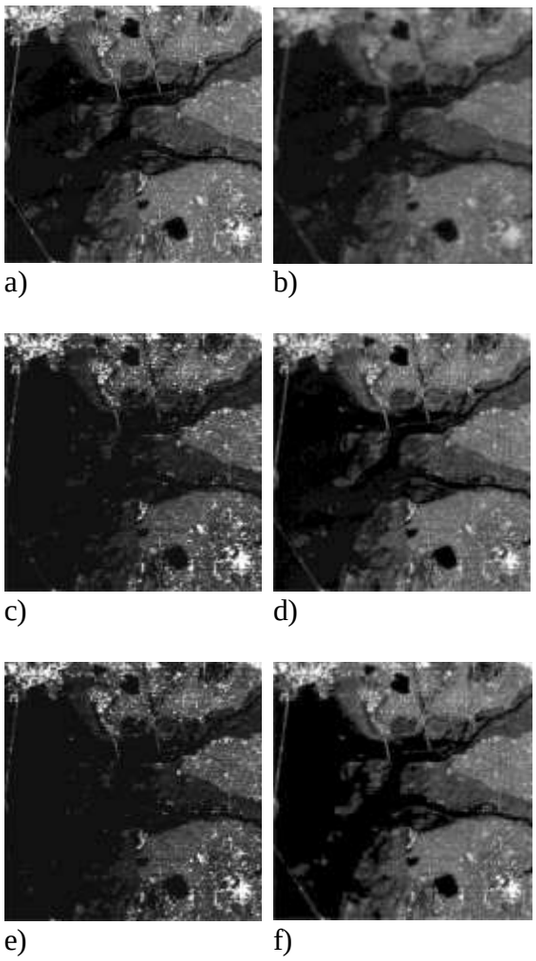

Figure 2 (a) Original 512x512-pixels test scene borrowed from the real-world high resolution SAR imagery ; (b) LR 512x512-pixels speckle corrupted radar image of the same scene formed with a simulated LR F-SAR system; model system parameters: triangular range PSF (the width at ½ of the peak value, κ_y = 10 pixels); Gaussian bell azimuth PSF (the width at ½ of the peak value, κ_x = 15 pixels); single-look scenario with the fully developed speckle, SNR = 0 dB; (c) 512x512-pixels image enhanced using the DEDR framework with the solution operator RASF, (3) with λ_1 = 1, λ_2 = 0 (convergence at I = 15, *PSNR* = 17.7208 dB); (d) 512x512-pixels image enhanced with the most prominent competing structured DEDR-POCS technique (3) with $\lambda_1 = \lambda_2 = 1$ (convergence at I = 10, *PSNR* = 22.6092 dB); (e) Fused image using DWT (Daubechies wavelet); (f) Fused image using MLP (with backpropation, three input neurons and one for output)

The MLP contain three input units and one output unit, with 90 hidden units. For comparison purposes, we also perform fusion using the DWT-based method mentioned earlier. The "daubechies" wavelet basis is used. Thus, the only way to analyze and compare the noise suppression and the pixel clarity is to perform the simulation experiments.

We must simulate the fractional SAR (F-SAR) imaging RS system with operational parameters similar to the comparative studies. The simulation results of enhancement of such F-SAR imagery applying different DEDR-POCS and RASF methods are reported in Figure 2. The test 512x512-pixel HR image Figure 2(a) borrowed from the real-world SAR imagey (Skymed, s.f.) relates to the hypothetical full focused SAR imaging mode. The 512x512-pixel LR speckle corrupted image of the same scene presented in Figure 2(b) corresponds to the single look F-SAR mode (quick look modality (2)) for the typical F-SAR operational scenario specifications, like the comparative previous studies. Figure 2(c) and 2(d) report the feature-enhanced radar imaging results obtained via the DEDR-POCS and RASF techniques.

In order to evaluate the quality of the high-resolution enhanced images, two metrics have been adopted: the peak signal-to-noise ratio (PSNR) as an extension of the mean squared error (MSE) and the structural similarity index (SSIM) (Hore & Ziou, 2010):

$$\mathrm{MSE}\left(\mathbf{b},\hat{\mathbf{b}}_{\mathrm{F}}\right)=\frac{1}{JK}\sum_{j=1}^{J}\ \sum_{k=1}^{K}\ \left(b_{jk}-\hat{b}_{F_{jk}}\right)^{2} \qquad (13)$$

Where $\mathbf{b}$ represents the original SSP frame and $\hat{\mathbf{b}}_{\mathrm{F}}$ is the fusion image approximation obtained through DWT fusion or MLP fusion.

$$\mathrm{PSNR\ [dB]}=10log_{10}\left\{\frac{1}{\mathrm{MSE}\left(\mathbf{b},\hat{\mathbf{b}}_{\mathrm{F}}\right)}\right\} \qquad (14)$$

$$\mathrm{SSIM}\left(\mathbf{b},\hat{\mathbf{b}}_{\mathrm{F}}\right)=\frac{\left(2\mu_{\mathbf{b}}\mu_{\hat{\mathbf{b}}_{\mathrm{F}}}+C_1\right)\left(2\sigma_{\mathbf{b}\hat{\mathbf{b}}_{\mathrm{F}}}+C_2\right)}{\left(\mu_{\mathbf{b}}{}^2+\mu_{\hat{\mathbf{b}}_{\mathrm{F}}}{}^2+C_1\right)\left(\sigma_{\mathbf{b}}{}^2+\sigma_{\hat{\mathbf{b}}_{\mathrm{F}}}{}^2+C_2\right)} \qquad (15)$$

Where μ_x is the mean intensity, σ_x is standard deviation and σ_{xy} is the covariance between the involved images.

ISSN 2444-5002

The comparative results are presented in Table 1. These results verify that the best perceptual fusion image performances regarding the PSNR $(\mathbf{b}, \hat{\mathbf{b}}_F)$ and SSIM$(\mathbf{b}, \hat{\mathbf{b}}_F)$ metrics are reached by the MLP fusion method.

	Test Case Comparative Metrics (average)	
	DWT (Daubechies)	**MLP**
PSNR	17.8571 dB	21.1645 dB
SSIM	O.6225	0.7998

Table 1 Comparative Metrics

In general, if the window size is too large, a particular window may contain two or more objects or information at the different distances and consequently will lead to a less clear image. On the other hand, using small window size may lead to the saw-tooth effect.

References

Eskicioglu, A., & Fisher, P. (1995). Image quality measures and their performance. IEEE Transactions on Communications, 43(12), 2959–2965. https://doi.org/10.1109/26.477498

Henderson, F. M., & Lewis, A. V. (1998). Principles and Applications of Imaging Radar, Manual of Remote Sensing (3ª ed.). N.Y, USA: Willey.

Hore, A., & Ziou, D. (2010). Image Quality Metrics: PSNR vs. SSIM. 2010 20th International Conference on Pattern Recognition, . https://doi.org/10.1109/icpr.2010.579

Hui Li, Manjunath, B., & Mitra, S. (1995). Multi-sensor image fusion using the wavelet transform. Proceedings of 1st International Conference on Image Processing,

Kulkarni, A. (2001). Computer Vision and Fuzzy-Neural Systems (Ed. rev.). N.J., USA: Prentice Hall.

Li, S., Kwok, J. T., & Wang, Y. (2002). Multifocus image fusion using artificial neural networks. Pattern Recognition Letters, 23(8), 985–997.

Li, S., Yang, B., & Hu, J. (2011). Performance comparison of different multi-resolution transforms for image fusion. Information Fusion, 12(2), 74–84. https://doi.org/10.1016/j.inffus.2010.03.002

Pajares, G., & Manuel de la Cruz, J. (2004). A wavelet-based image fusion tutorial. Pattern Recognition, 37(9), 1855–1872.

Shkvarko, Y. (2010). Unifying Experiment Design and Convex Regularization Techniques for Enhanced Imaging With Uncertain Remote Sensing Data—Part I: Theory. IEEE Transactions on Geoscience and Remote Sensing, 48(1), 82–95. https://doi.org/10.1109/tgrs.2009.2027695

Shkvarko, Y., Tuxpan, J., & Santos, S. (2011). Dynamic Experiment Design Regularization Approach to Adaptive Imaging with Array Radar/SAR Sensor Systems. Sensors, 11(5), 4483–4511.

Shutao Li, & Bin Yang, (2010). Hybrid Multiresolution Method for Multisensor Multimodal Image Fusion. IEEE Sensors Journal, 10(9), 1519–1526.

Skymed, C. O. S. M. O. (s.f.). COSMO-SkyMed / CUGS. Recuperado 5 mayo, 2017, de http://www.cosmo-skymed.it.

Torres, D. G., Tuxpan, J., & Yanez, I. (2014). Spatial spectrum pattern estimation based on the DEDR-TV extended approach for fractional SAR imagery enhancement. 2014 International Conference on Electronics, Communications and Computers (CONIELECOMP), . https://doi.org/10.1109/conielecomp.2014.6808560

Yang, Y., Park, D. S., Huang, S., & Rao, N. (2010). Medical Image Fusion via an Effective Wavelet-Based Approach. EURASIP Journal on Advances in Signal Processing, 2010(1). https://doi.org/10.1155/2010/579341

Zheng, Y., Essock, E. A., Hansen, B. C., & Haun, A. M. (2007). A new metric based on extended spatial frequency and its application to DWT based fusion algorithms. Information Fusion, 8(2), 177–192.

ISSN 2444-5002